UC Berkeley
UC Berkeley Previously Published Works

Title

Enhanced Carbon Dioxide Capture from Diluted Streams with Functionalized Metal-Organic Frameworks.

Permalink

Journal

Authors

Gładysiak, Andrzej
Song, Ah-Young
Vismara, Rebecca
et al.

Publication Date

DOI

Article

Enhanced Carbon Dioxide Capture from Diluted Streams with Functionalized Metal−Organic Frameworks

Andrzej Gładysiak,* Ah-Young Song, Rebecca Vismara, Madison Waite, Nawal M. Alghoraibi, Ammar H. Alahmed, Mourad Younes, Hongliang Huang, Jeffrey A. Reimer, and Kyriakos C. Stylianou*
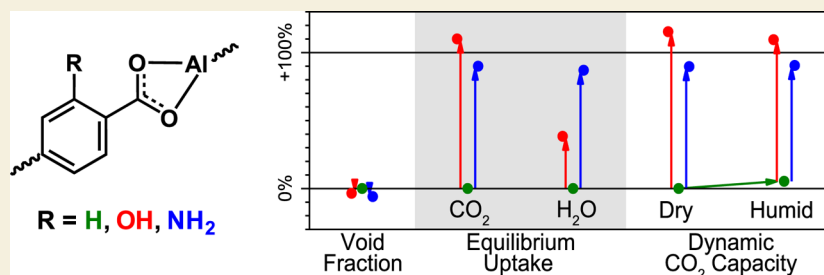
Read Online

ACCESS | Metrics & More | Article Recommendations | Supporting Information

ABSTRACT: Capturing carbon dioxide from diluted streams, such as flue gas originating from natural gas combustion, can be achieved using recyclable, humidity-resistant porous materials. Three such materials were synthesized by chemically modifying the pores of metal−organic frameworks (MOFs) with Lewis basic functional groups. These materials included aluminum 1,2,4,5-tetrakis(4-carboxylatophenyl) benzene (Al-TCPB) and two novel MOFs: Al-TCPB(OH), and Al-TCPB(NH$_2$), both isostructural to Al-TCPB, and chemically and thermally stable. Single-component adsorption isotherms revealed significantly increased CO$_2$ uptakes upon pore functionalization. Breakthrough experiments using a 4/96 CO$_2$/N$_2$ gas mixture humidified up to 75% RH at 25 °C showed that Al-TCPB(OH) displayed the highest CO$_2$ dynamic breakthrough capacity (0.52 mmol/g) followed by that of Al-TCPB(NH$_2$) (0.47 mmol/g) and Al-TCPB (0.26 mmol/g). All three materials demonstrated excellent recyclability over eight humid breakthrough-regeneration cycles. Solid-state nuclear magnetic resonance spectra revealed that upon CO$_2$/H$_2$O loading, H$_2$O molecules do not interfere with CO$_2$ physisorption and are localized near the Al-O(H) chain and the −NH$_2$ functional group, whereas CO$_2$ molecules are spatially confined in Al-TCPB(OH) and relatively mobile in Al-TCPB(NH$_2$). Density functional theory calculations confirmed the impact of the adsorbaphore site between of two parallel ligand-forming benzene rings for CO$_2$ capture. Our study elucidates how pore functionalization influences the fundamental adsorption properties of MOFs, underscoring their practical potential as porous sorbent materials.

KEYWORDS: pore functionalization, CO$_2$ capture, H$_2$O isotherms, breakthrough curves, humid flue gas, adsorbaphore

INTRODUCTION

Postcombustion carbon dioxide (CO$_2$) capture is a viable solution to mitigate CO$_2$ emissions from large point sources.[1] In the U.S., generation of electricity in conventional power plants is currently responsible for 31% of all CO$_2$ emissions.[2] Coal was traditionally the primary energy source for electricity generation; but its use has declined since 2008 as it has been replaced by natural gas.[3] Flue gas emanating from natural gas-fired power plants contains very small amounts of SO$_2$ and NO$_x$, thus posing less of immediate environmental concern compared to flue gas originating from coal-fired power plants.[4] However, the CO$_2$ content in the natural gas-generated flue gas (4 vol % CO$_2$) is significantly lower than that from coal, making CO$_2$ capture from these diluted streams more challenging.[4] Currently, aqueous alcoholamine scrubbing is the only mature and efficient postcombustion CO$_2$ capture technology.[5] However, it is burdened by high parasitic energy

requirements and the environmental concerns associated with high-temperature alcoholamine degradation.[6,7] To address these issues, less energy-demanding solid materials that rely on CO$_2$ adsorption have been developed. While the thermal regeneration of these porous materials is easy, they tend to adsorb not only CO$_2$ but also large amounts of water vapor present in postcombustion flue gas.[8] Therefore, designing porous materials that selectively adsorb CO$_2$ while excluding H$_2$O remains a major synthetic challenge.

Figure 1. (a) Molecular structure of the H₄TCPB ligand and its functionalized analogs. DFT-relaxed structure of the Al-TCPB MOF visualized in the ball-and-stick mode viewed along [001] (b) and [010] (c). The same structure visualized in the sphere packing mode viewed along [001] (d) and [010] (e). Atom color code: light blue, Al; gray, C; red, O; white, H.

Metal−organic frameworks (MOFs) stand out among porous materials for postcombustion CO_2 capture due to their intrinsic modularity and excellent structural tunability, allowing the design of pore landscapes that favor CO_2 adsorption.[9] Among these, fluorinated narrow-pore NbOF-FIVE-1-Ni is one of the most promising materials, with a CO_2 uptake of 2.2 mmol/g at 298 K and 40 mbar CO_2, and a heat of adsorption of 50 kJ/mol, presenting a balanced compromise between uptake and regeneration energy.[10] Similarly, fluorinated MOFs of the SIFSIX-3 family exhibit comparable properties.[11−13] In contrast, N,N'-dimethylethylenediamine (mmen)-appended Mg_2(dobpdc) has a higher uptake under the same conditions (2.9 mmol/g) but also a higher heat of adsorption (71 kJ/mol) making the thermal regeneration more energy-intensive.[14]

MOFs offer a unique platform to study structure−property relationships as by preparing pairs of isostructural MOFs that differ by a single structural feature, insights can be gained on the impact of that specific structural alteration. Several synthetic strategies to enhance CO_2 capture have been developed through this approach.[15−18] For example, in the MOF families such as M-MOF-74,[19] mmen-M_2(dobpdc),[20]

and M(L)(bpy),[21] the nature of the metal center dictates the shape of the CO_2 adsorption isotherm as well as the CO_2 uptake. In HKUST-1, the attachment of H_2O molecules to the metal clusters results in an increase in CO_2 uptake.[22] A similar phenomenon occurs with alcohol molecules in InOF-1 and MIL-53(Al), although in these MOFs, the molecules are confined in the pore space through noncovalent interactions.[23,24] Covalently attaching hydroxide anions to the metal centers of MAF-X25 and MAF-X27 significantly increased CO_2 uptake at low pressures, with heats of adsorption reaching up to 124 kJ/mol.[25] Additionally, comparing chemically identical frameworks, one interpenetrated and one not, demonstrated that interpenetration enhanced CO_2 uptake by maintaining a relatively low heat of adsorption.[13] Similarly, pressure-, heat-, or light-induced phase transitions in coordination networks can lead to phases endowed with enhanced CO_2 capture capabilities.[26−32] Carbon dioxide adsorption on MOFs can also be improved by engineering composites on supports such as graphite oxide or carbon nanotubes.[33−36]

One of the most effective strategies for enhancing CO_2 capture in MOFs is ligand functionalization.[15−18] By

substituting H atoms in the ligand structure with more electronegative atoms such as N, O, or F, the polarizability of the ligand increases. This, in turn, enhances dispersion interactions with the quadrupole moment of the CO_2 molecules when exposed to the MOF pores. Additionally, pores can be modified postsynthetically by grafting amine molecules onto the open metal sites,[37] allowing CO_2 to interact through chemisorption, forming carbamate or bicarbonate species.[37] Both pre- and postsynthetic functionalization methods have demonstrated significant improvements in CO_2 capture at 40 mbar and 298 K, as exemplified by numerous MOFs listed in Table S1. Presynthetic functionalization with an $-NH_2$ group can significantly increase CO_2 uptake, as demonstrated by MIL-101(Cr),[38] which exhibits an order of magnitude increase; however, absolute values typically remain below 0.5 mmol/g. Amine-grafted MOFs can achieve higher CO_2 capture under similar conditions, but their heats of adsorption are notably high. Additionally, as illustrated in Table S2, MOF functionalization not only boosts CO_2 sorption but can also increase the adsorption of H_2O vapor, which can be detrimental to performance in humid conditions.[39,40]

We have recently intensified our research efforts toward the development of novel humidity-resistant CO_2 capture materials. Indeed, we discovered a preferred CO_2 adsorption site, an adsorbaphore, in a hydrophobic pocket sandwiched in between of two pyrene cores separated by ∼7 Å in Al-PyrMOF. This site exclusively hosts CO_2 and repels H_2O molecules, enabling Al-PyrMOF to capture the same amount of CO_2 under both dry and humid conditions.[41] A similar versatility was displayed by Al-MIL-120, a member of the Al-MOF family well-known for their paramount chemical stability,[42-44] where the spacing between adjacent pyromellitate rings is 4.78 Å.[45] In our transition-metal-based $Ni_3(pzdc)_2(ade)_2$, the CO_2 uptake under humid conditions was 23% lower than under the dry conditions; however, the material exhibited interesting catalytic properties.[46]

In this study, we introduce aluminum 1,2,4,5-tetrakis(4-carboxylatophenyl)benzene (Al-TCPB) as a novel humidity-resistant CO_2 capture adsorbent. The synthesis and solid-state characterization of this material is followed by a thorough investigation of its potential for CO_2 capture. Additionally, we report the synthesis of two novel Al(III) MOFs based on the H_4TCPB ligand chemically functionalized with hydroxy and amino groups. The sorption properties of Al-TCPB, Al-TCPB(OH), and Al-TCPB(NH_2) are compared and analyzed using spectroscopic data and density functional theory (DFT) calculations.

■ RESULTS AND DISCUSSION

The orthorhombic (space group $Cmmm$) structure of $Al_2(OH)_2(TCPB)$, also known as CAU-9 or Al-BMOF, and here referred to as Al-TCPB, was previously determined from powder X-ray diffraction (PXRD) data.[47] In Al-TCPB, alternating Al atoms and bridging hydroxide ligands extend along [010], forming the backbone of the structure. These mutually parallel chains are connected in the (010) plane with $TCPB^{4-}$ ligands (Figure 1a), with each of their six carboxylate O atoms coordinating to a distinct Al atom (Figure 1b). Thus, the one-dimensional inorganic chains can be viewed as composed of corner-sharing distorted AlO_6 octahedra. Within the ligands, the distal phenylene rings are perpendicular to the

central 4-substituted benzene ring cores, which in turn are stacked along [010] (Figure 1c).

The structure of Al-TCPB was relaxed using DFT calculations, and the resulting model was consistent with the previously reported structure.[47] Subsequently, structural models Al-TCPB(OH) and Al-TCPB(NH_2), incorporating hydroxylated and aminated ligands, respectively (Figure 1a), were constructed and relaxed using DFT. The models also converged to the respective isostructures. All three MOFs feature three types of 1-dimensional pores: pore I, lined with the benzene cores of the $TCPB^{4-}$ ligands separated by 6.64 Å, running perpendicular to the Al-O(H) chains (Figure 1d); pore II, lined with distal phenylene rings of the $TCPB^{4-}$ ligands, running parallel to the Al-O(H) chains; and pore III, having the same characteristics as pore II, but also exposed to chain-forming hydroxides (Figure 1e). Numerical analysis of the DFT-relaxed models (see the Supporting Information for further detail), provided the sizes of each pore and the void-volume fractions. As shown in Table 1, the introduction of the −OH or the −NH_2 groups into the Al-TCPB structure slightly reduces the size of pore II, while the sizes of the other two pores remain unchanged.

Table 1. Pore Sizes and Void Volume Fractions in the DFT-Relaxed Structures of Al-TCPB and Its Analogs

	pore I size (Å)	pore II size (Å)	pore III size (Å)	void fraction (%)
Al-TCPB	4.44	5.30	6.60	48.8
Al-TCPB(OH)	4.44	5.23	6.59	47.1
Al-TCPB(NH_2)	4.44	5.18	6.59	45.9

Al-TCPB, Al-TCPB(OH), and Al-TCPB(NH_2) were successfully synthesized from the respective ligands (Figure S1) and an Al(III) salt in water and *N,N*-dimethylformamide (DMF). While Al-TCPB was obtained on the multigram scale, the scaleup of Al-TCPB(OH) and Al-TCPB(NH_2) was hindered by the limited availability of the respective ligand. PXRD analysis of these crystalline solids confirmed the identity of Al-TCPB and showed that Al-TCPB(OH) and Al-TCPB(NH_2) are isostructural to Al-TCPB (Figure 2).
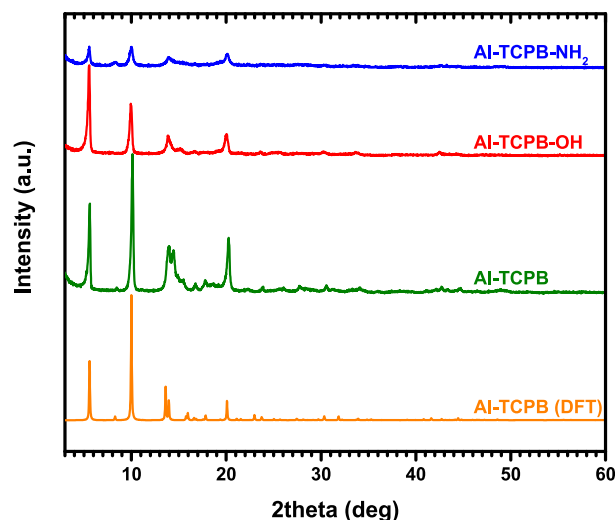

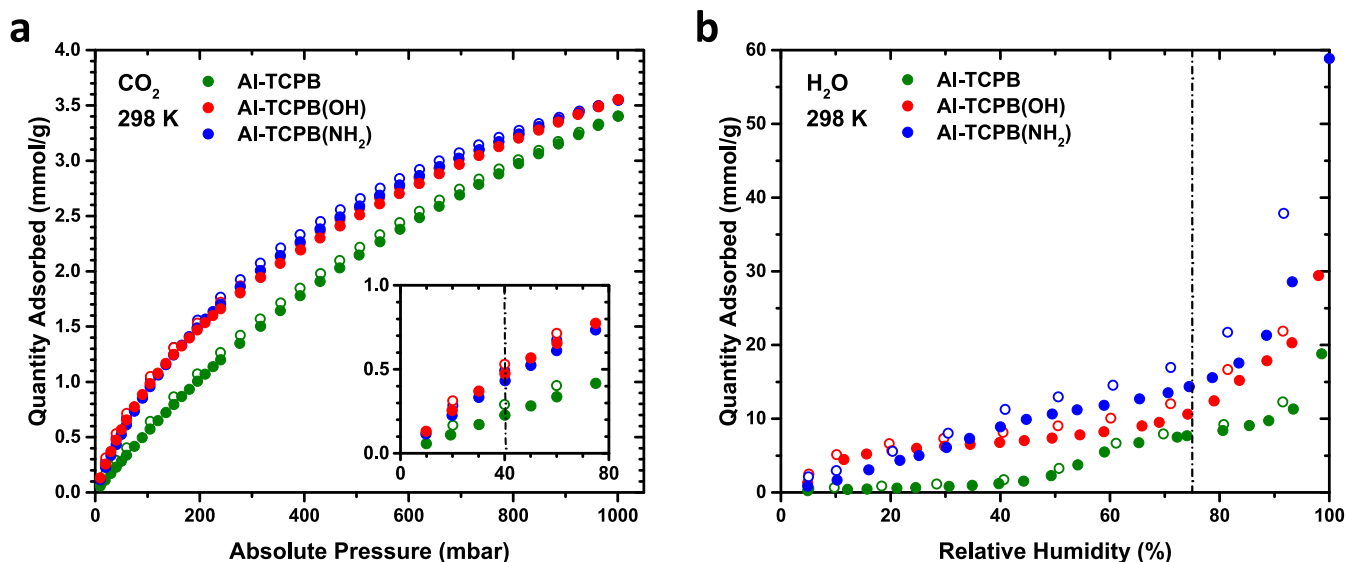**Figure 2.** PXRD patterns of Al-TCPB and its analogs compared to that calculated for the DFT-relaxed Al-TCPB structure.

Figure 3. (a) CO_2 and (b) H_2O vapor adsorption isotherms of Al-TCPB and its analogs at 298 K. Full symbols denote adsorption, while the empty ones denote desorption. The conditions of interest for the postcombustion carbon capture (CO_2 absolute pressure of 40 mbar; 75% RH) have been marked with dashed-dotted lines.

Thermogravimetric analysis (Figure S2) indicated that the temperature of decomposition was 514 °C for Al-TCPB, 351 °C for Al-TCPB(OH), and 386 °C for Al-TCPB(NH_2). These temperature points are preceded by sample drying taking place at temperatures below 80 °C, and by the loss of the occluded solvent taking place from 80 to 300 °C in all the three materials. The chemical stability of Al-TCPB and its analogs was tested by immersing them in water for 3 h and exposing them to nitric acid fumes for 3 h. Their PXRD patterns confirmed their stability under these conditions (Figures S3−S5). Solvent exchange followed by outgassing yielded fully activated materials that retained their crystallinity (Figures S3−S5). The PXRD peaks of the Al-TCPB samples that underwent differing treatment (as-made, activated, H_2O-soaked, HNO_3-exposed) all matched the DFT-simulated pattern well (Figure S3), suggesting this material is very robust. Conversely, in Al-TCPB(OH) and Al-TCPB(NH_2), the prominent 200, 201, 110, 401, and 402 PXRD peaks underwent slight shifts with respect to their predicted positions (Figures S4 and S5) prompting some extent of flexibility of these materials, akin to that exhibited by CALF-20,[48,49] and Ca-TBAPy.[50] In the Fourier transform infrared (FT-IR) spectrum of Al-TCPB, a broad band at 3300 cm^{-1}, associated with the O−H stretching of H_2O molecules occluded in the pores upon synthesis, disappeared upon activation (Figure S6). In contrast, Al-TCPB(OH) and Al-TCPB(NH_2) exhibited FT-IR bands at 3250 and 3400 cm^{-1}, well pronounced both before and after activation, and corresponding to the O−H and N−H stretching of their respective functional groups (Figures S7 and S8). Additionally, all three materials showed the disappearance of the C═O stretching band at ~1670 cm^{-1}, indicating the release of occluded DMF solvent molecules.

The gas adsorption properties of the activated samples of the Al-TCPB materials were investigated. At 77 K, all three analogs exhibited type I nitrogen isotherms (Figure S9), which are characteristic of microporous materials. The Brunauer−Emmett−Teller surface areas for Al-TCPB, Al-TCPB(OH), and Al-TCPB(NH_2) were 1149(2), 831.0(18), and 1078(2) m^2/g, respectively (Table S3). CO_2 adsorption at 298 K also

displayed type I isotherms, with Al-TCPB(OH) and Al-TCPB(NH_2) outperforming Al-TCPB across all pressures (Figure 3a). The CO_2 uptakes of the Al-TCPB materials at 40 mbar and 298 K, summarized in Table 2, were higher than

Table 2. Equilibrium Adsorbed Amounts of CO_2 and H_2O at Conditions Relevant to Post-Combustion CO_2 Capture Derived from the Respective 298 K Adsorption Isotherms

	CO_2 uptake at 40 mbar (mmol/g)		H_2O uptake at 75% RH (mmol/g)	
	adsorption	desorption	adsorption	desorption
Al-TCPB	0.227	0.291	7.69	8.58
Al-TCPB(OH)	0.474	0.530	10.6	14.3
Al-TCPB(NH_2)	0.432	0.493	14.3	19.3

those of the majority of presynthetically modified MOFs (Table S1), but lower than that of CALF-20, a MOF currently exploited in the industry (1.8 mmol/g),[51] and lower than those of the majority of postsynthetically modified MOFs (Table S1). CO_2 adsorption isotherms recorded at 293 (Figure S10), 298, and 303 K (Figure S11) enabled the determination of the isosteric heat of CO_2 adsorption, which was 24 kJ/mol for Al-TCPB, and 30 kJ/mol for both Al-TCPB(OH) and Al-TCPB(NH_2) (Figure S12). The adsorption of H_2O vapor revealed distinct behaviors among Al-TCPB and its analogs. At 298 K, Al-TCPB(OH) exhibited a type I H_2O vapor isotherm, while the isotherms for Al-TCPB and Al-TCPB(NH_2) featured inconspicuous steps (Figure 3b), prompting a degree of cooperativity in H_2O adsorption,[52,53] namely, that the H_2O adsorption in one type of pore may facilitate the H_2O adsorption in another type of pore. The H_2O vapor adsorption on Al-TCPB was reversible, whereas Al-TCPB(OH) and Al-TCPB(NH_2) exhibited minimal hysteresis in their isotherms (Figure 3b). Compared to another hydrophobic MOF, CALF-20,[51] the H_2O vapor uptake of Al-TCPB is much lower at relative humidities lower than 50%, comparable at the intermediate values of RH, and surpasses CALF-20 only at relative humidities greater than 80%. In turn, the H_2O vapor

uptakes of Al-TCPB(OH) and Al-TCPB(NH$_2$) are greater than those of CALF-20 across the entire RH range. Interestingly, despite significant differences in their H$_2$O vapor uptakes, all three Al-TCPB materials demonstrated nearly identical macroscopic hydrophilicity, as indicated by contact angle measurements (Figure S13). Furthermore, Al-TCPB and its analogs maintained stability upon H$_2$O adsorption (Figure S14), thus they are among the MOFs with high H$_2$O uptakes and high hydrolytic stabilities.[54−56]

The performance and stability of porous materials under operating conditions are important considerations for effective CO$_2$ capture. Our materials were tested under conditions pertinent to CO$_2$ capture from flue gas produced by natural gas-powered power plants, including CO$_2$ partial pressure of 40 mbar, total pressure of 1 bar, temperature of 25 °C, and, when considering humidity, 75% relative humidity (RH), corresponding to $p/p^0 = 0.75$. These conditions were chosen to align with our laboratory capabilities and ensure comparability with literature data. Single-gas adsorption analysis of CO$_2$ uptakes at 40 mbar and H$_2$O uptakes at 75% RH (Table 2) reveals that, at 298 K, Al-TCPB and its analogs exhibit higher selectivity toward H$_2$O over CO$_2$ under thermodynamic equilibrium conditions. However, as inferred from quantities adsorbed at low pressures, the adsorption of H$_2$O vapor on activated Al-TCPB and its analogs takes place at a significantly slower rate compared to that of CO$_2$ (Figure S15). Moreover, single-component isotherms completely ignore the likelihood of competition between different adsorbates for the same adsorption sites. To address these limitations, dynamic breakthrough curves were measured using a fixed-bed reactor setup (Figure S16). Samples were enclosed in a tubular column, activated at 150 °C, and conditioned in a stream of dry N$_2$ at 25 °C. This conditioning must inevitably have contributed to some adsorption of N$_2$ on the solid material surface. At the outset of each breakthrough measurement, the gas flowing through the column was switched to 4/96 CO$_2$/N$_2$, and the outlet gas composition was recorded with a mass spectrometer. CO$_2$ subsequently replaced N$_2$ on the surface of the Al-TCPB materials as deduced from the shape and position of the CO$_2$ and N$_2$ breakthrough curves—all the experimental CO$_2$ signals lay below the blank, while all the experimental N$_2$ signals lay above the blank (Figures S17−S19). The CO$_2$ capacity of Al-TCPB and its analogs, calculated by numerically integrating the CO$_2$ breakthrough curves, remained unaffected by the presence of humidity in the simulated flue gas stream. Al-TCPB(OH) exhibited the highest average CO$_2$ breakthrough capacity of 0.52 mmol/g, surpassing Al-TCPB(NH$_2$) (0.47 mmol/g) and Al-TCPB (0.26 mmol/g) across 8 cycles, each comprising a CO$_2$ capture under humid conditions and subsequent thermal regeneration (Figure 4 and Table S4). Importantly, the sequence of CO$_2$ breakthrough capacities (Table S4)—Al-TCPB < Al-TCPB(NH$_2$) < Al-TCPB(OH)— was consistent with the sequence of CO$_2$ uptake inferred from the respective CO$_2$ adsorption isotherms (Table 2). Flushing the fixed-bed reactor with a humid N$_2$ stream for 3 h resulted in a complete loss of CO$_2$ sorption properties in all materials. However, intense thermal regeneration subsequently restored the CO$_2$ breakthrough capacity over two dry-gas and two humid-gas capture-regeneration cycles (Figure 4 and Table S4). These findings confirm that while equilibrium uptake of H$_2$O vapor is greater than that of CO$_2$ on Al-TCPB and its analogs (Table 2), the adsorption of CO$_2$ is preferred kinetically, allowing for its capture under humid conditions
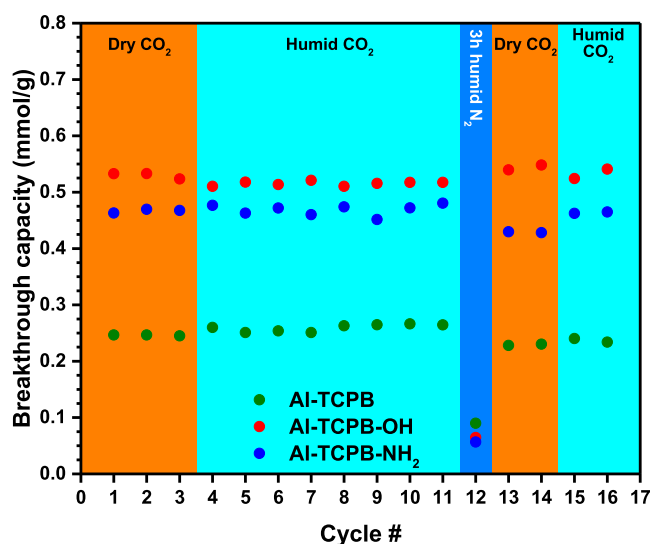

Figure 4. Dynamic breakthrough CO$_2$ capacity of Al-TCPB and its analogs in a fixed-bed reactor fed with 4/96 (v/v) CO$_2$/N$_2$ gas mixture at 298 K.

(Figure 4 and Table S4). A similarly slow H$_2$O adsorption kinetics has recently been reported to allow for humid-gas CO$_2$ capture in TIFSIX-3-Ni.[57] The CO$_2$ breakthrough capacities reported here are lower than those of the 2-ampd-Mg$_2$(dobpdc) MOF (2.4(2) mmol/g, dry and humid 4/96 CO$_2$/N$_2$ gas mixture)[58] and the 2-ampd-Mg$_2$(dobpdc)/PES hollow fiber (2.5 mmol/g$_{MOF}$, dry 4.4/4.5/91 CO$_2$/He/N$_2$ gas mixture);[59] however, the excellent recyclability of Al-TCPB, Al-TCPB(OH), and Al-TCPB(NH$_2$) after capture under humid conditions sets them apart. In this context, Al-TCPB and its analogs exhibit performance comparable to kag-MOF-1, which retained a dynamic breakthrough CO$_2$ capacity of 0.57 mmol/g (2.5 wt %) with a 10/90 CO$_2$/N$_2$ gas mixture, even after regeneration under humid (75% RH) conditions. This is noteworthy given the higher H$_2$O vapor uptake (11.7 wt %) at 75% RH compared to the CO$_2$ uptake (3.5 wt %) at 100 mbar derived from single-component 298 K isotherms.[60]

Solid-state NMR spectroscopy was employed to investigate the sorption behavior of Al-TCPB and its analogs under dynamic conditions relevant to humid CO$_2$ capture. All C atoms that were not related by symmetry were successfully assigned in the ^{13}C solid-state NMR spectra of Al-TCPB, Al-TCPB(OH), and Al-TCPB(NH$_2$), revealing the most significant downfield shift for the C atom directly bound to either the −OH or the −NH$_2$ functional group (Figure S20). Subsequently, the samples were activated in situ and dosed with pure ^{13}CO$_2$ humidified up to 75% RH. In the ^{1}H solid-state NMR spectrum of Al-TCPB measured under these conditions, the peak at 2.8 ppm has been associated with the H atom of the Al-bound hydroxide (Figure S21). Interestingly, prolonged exposure to humidity caused a downfield shift and a broadening of this peak (Figure S21), suggesting interaction of H$_2$O vapor molecules with the Al-O(H) chains, possibly through hydrogen bonds. In turn, ^{1}H−^{13}C heteronuclear correlation (HETCOR) NMR spectra recorded under the same conditions revealed that the ^{13}C resonance associated with the C atom bound directly to the −NH$_2$ functional group in Al-TCPB(NH$_2$) correlates with the ^{1}H resonance of the H atoms of H$_2$O vapor molecules (Figure S22). This correlation suggests an interaction between these two species, while

similar correlations were not observed in Al-TCPB(OH) (Figure S23) and Al-TCPB (Figure S24), likely due to weaker $OH_2 \cdots C(-OH)$ and $OH_2 \cdots C(-H)$ interactions. Furthermore, the peak at 124.5 ppm in the ^{13}C spectra, observed after dosing with pure $^{13}CO_2$ humidified up to 75% RH, exhibited a significant intensity reduction upon prolonged spinning (Figure S25), indicating its association with physisorbed $^{13}CO_2$. The position of this peak remained consistent across the Al-TCPB analog series (Figure 5); however, its line width
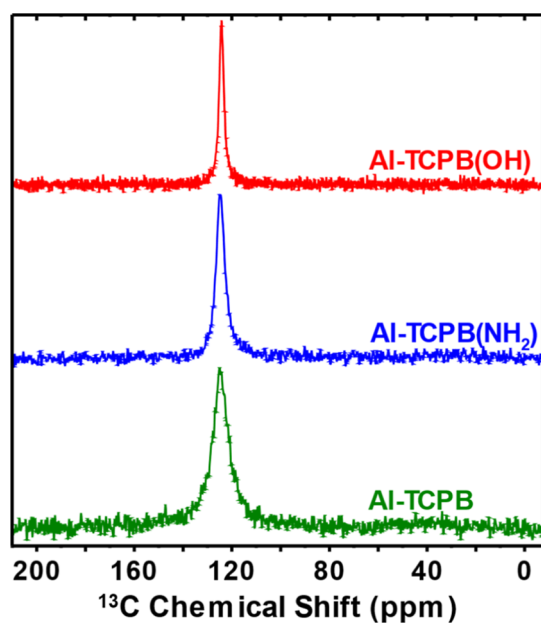
Figure 5. Physisorbed $^{13}CO_2$ peak in the ^{13}C solid-state NMR spectra recorded upon wet (75% RH) pure $^{13}CO_2$ dosing. Details of this peak are reported in Table 3.

followed the trend Al-TCPB(OH) < Al-TCPB(NH$_2$) < Al-TCPB (Table 3), which may be indicative of significant

Table 3. Position and Width of the Physisorbed $^{13}CO_2$ Peak in the ^{13}C Solid-State NMR Spectra Recorded upon Dosing with Pure $^{13}CO_2$ Humidified to 75% RH with H_2O or D_2O

	δ ^{13}C (ppm)	$^{13}CO_2/H_2O$ dosing linewidth (Hz)	$^{13}CO_2/D_2O$ dosing linewidth (Hz)
Al-TCPB(OH)	124.460(5)	415(3)	374.3(12)
Al-TCPB(NH$_2$)	124.790(7)	753(5)	798(4)
Al-TCPB	124.790(16)	1412(12)	1383(10)

mobility of CO_2 molecules in Al-TCPB and their spatial confinement, possibly facilitated by an array of H-bonds, in Al-TCPB(OH). The condition of CO_2 molecules in Al-TCPB-(NH$_2$) is thought to be intermediate. When D_2O (invisible in NMR) was used instead of H_2O to humidify the $^{13}CO_2$ gas, the $^{13}CO_2$ peak position remained unchanged, with only slight changes in line width observed (Table 3). The minor variations in peak line width may indicate a minimal impact of water molecule protons on the dipolar interactions between water and CO_2. This suggests that water vapor likely does not significantly interact with physisorbed CO_2.

Intermolecular interactions involving CO_2, H_2O, and Al-TCPB and its analogs were further investigated computationally. Using DFT, we introduced a CO_2 molecule into three

distinct sites within the pores of Al-TCPB, Al-TCPB(OH), and Al-TCPB(NH$_2$), and the resulting structures were relaxed. An analogous procedure was applied for three H_2O sites, allowing us to assess the orientation changes sustained by guest molecules, and the energetics of host−guest interactions. The geometries of the CO_2 and H_2O molecules introduced in silico underwent very subtle position and orientation change upon DFT relaxation (Table S5). As shown in Figure 6, which reports exemplary optimized geometries for Al-TCPB(OH), CO_2 molecules stayed parallel to TCPB^{4-} benzene cores when adsorbed in pore I, and parallel to the Al-O(H) chains when in pore II and III, respectively. In turn, H_2O molecules tilted to maximize O−H$\cdots$O and O−H$\cdots\pi$ interactions (Figure 6). The CO_2−MOF and H_2O−MOF binding energies are charted in Table 4. It follows that CO_2 interacts preferentially with Al-TCPB and its analogs within their pore I, which is delimited by mutually parallel TCPB^{4-} central benzene rings constituting the CO_2 adsorbaphore. The CO_2−Al-TCPB(OH) interaction is the strongest and is followed by the CO_2−Al-TCPB(NH$_2$) and the CO_2−Al-TCPB interactions. In turn, H_2O interacts preferentially with Al-TCPB and Al-TCPB(NH$_2$) within their pore I, and with Al-TCPB within pore III, the latter being lined with distal TCPB^{4-} phenylene rings and hydroxides forming the Al-O(H). Interestingly, Al-TCPB and Al-TCPB(OH) interact more strongly with H_2O than they do with CO_2, while the difference between the H_2O−Al-TCPB(NH$_2$) and the CO_2−Al-TCPB(NH$_2$) interactions is modest (Table 4). This result can explain the preference of our materials adsorbing H_2O over CO_2 at the stage of thermodynamic equilibrium (compare with Table 2), to which DFT calculations commonly apply. However, when considering only the adsorbaphore of pore I, the preference of CO_2 adsorption in Al-TCPB(OH) and, to some extent, in Al-TCPB(NH$_2$) is evident (Table 4). We reason that even though the −OH groups are not exposed to pore I in Al-TCPB(OH), they increase the overall polarizability of the ligand, enhancing dispersive interactions with CO_2 within that pore. Our DFT calculations offer a tempting explanation why Al-TCPB(OH) showed the highest CO_2 breakthrough capacity unaffected by the presence of humidity.

◼ CONCLUSIONS

Structural modularity of MOFs allows for rational tuning of their functional properties to a much greater extent than in other classes of porous materials. We investigated the impact of the change of a single structural parameter, namely, the ligand functionalization in Al-TCPB, on the prospect of the resultant materials for postcombustion carbon dioxide capture. Core properties of the materials decorated with −OH or −NH$_2$ functional groups, such as pore size, crystallinity, and hydrolytic stability, remained unaltered with respect to the parent Al-TCPB material. However, the adsorption properties of the functionalized materials were greatly enhanced: Al-TCPB(OH) and Al-TCPB(NH$_2$) exhibited increased CO_2 and H_2O vapor uptakes, as evidenced by adsorption isotherms, and higher CO_2 capacities under dynamic conditions compared to Al-TCPB. Importantly, all three analogs maintained their performance under simulated flue gas conditions (25 °C, 1 bar, 4/96 CO_2/N_2 gas mixture), unaffected by the presence of 75% RH in the analysis gas stream, as evidenced by their consistent CO_2 breakthrough capacity over 8 CO_2 capture-regeneration cycles, underscoring their stability under carbon capture process conditions. Furthermore, even after humidification
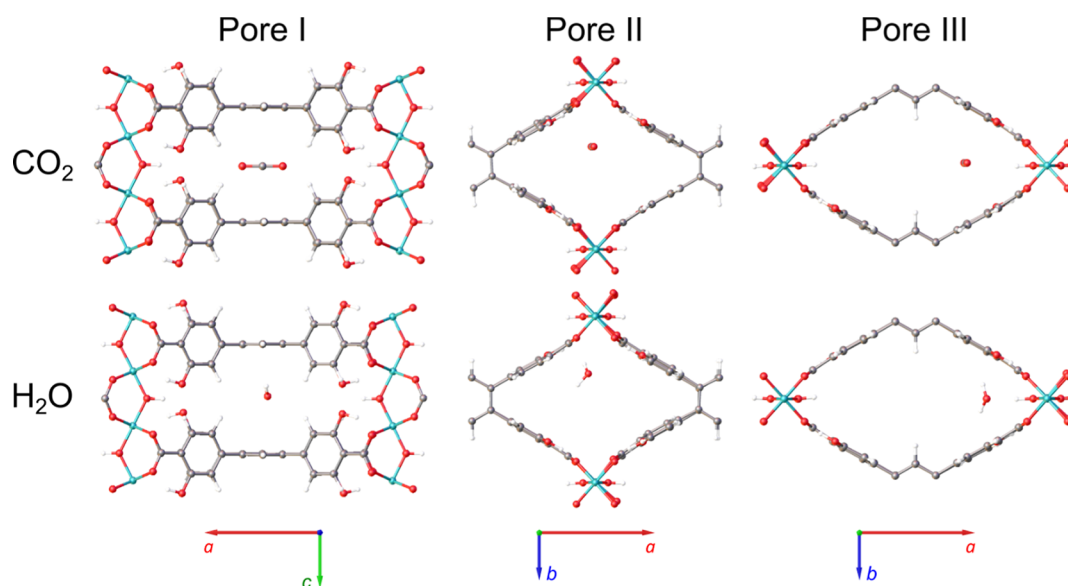
Figure 6. DFT-calculated adsorption sites and preferred geometric orientations of CO_2 and H_2O molecules adsorbed within the three pores of Al-TCPB(OH).

Table 4. DFT-Calculated Binding Energies of CO_2 and H_2O Adsorbed in Al-TCPB, Al-TCBP(OH), and Al-TCPB(NH$_2$) [a]

	CO_2			H_2O		
	pore I	pore II	pore III	pore I	pore II	pore III
Al-TCPB	**−34.56**	−33.23	−32.36	**−39.84**	−31.73	−27.86
Al-TCPB(OH)	**−47.66**	−41.32	−28.67	−35.85	−30.51	**−56.82**
Al-TCPB(NH$_2$)	**−41.85**	−41.15	−21.76	**−40.18**	−33.47	−25.18

[a]Values in kJ/mol.

for 3 h, these materials regained their sorption properties upon subsequent regeneration at 150 °C. Solid-state NMR spectra recorded upon wet (75% RH) $^{13}CO_2$ dosing revealed preferential interactions between H_2O molecules and Al-O(H) chains in Al-TCPB, and between H_2O molecules and the carbon atoms directly bound to the −NH$_2$ functional group in Al-TCPB(NH$_2$). Analysis of the physisorbed $^{13}CO_2$ peak line width in ^{13}C solid-state NMR spectra, recorded upon dosing with humidified $^{13}CO_2$, showed that CO_2 molecules are mobile in Al-TCPB and less so in Al-TCPB(OH), and that the presence of H_2O vapor does not significantly influence the physisorption of CO_2. An explanation why CO_2 adsorbs preferentially in Al-TCPB(OH) was further offered by DFT calculations. Al-TCPB(OH) has therefore been postulated as a functional material capable of capturing CO_2 from diluted and humid sources, although its scaleup and deployment will require further investigation. Additionally, the robustness of Al-TCPB, the flexibility of Al-TCPB(OH) and Al-TCPB(NH$_2$), both mentioned here only briefly, await further examination to decipher the influence of these structural phenomena on the CO_2 capture possibilities. Ongoing research in our laboratory continues to explore CO_2 capture using novel, aromatic-adsorbaphore-functionalized Al-MOFs.

■ ASSOCIATED CONTENT

ⓢ Supporting Information

The Supporting Information is available free of charge at https://pubs.acs.org/doi/10.1021/jacsau.4c00923.

Experimental procedure and computational details; tabulated literature survey data; TGA thermograms,

PXRD patterns, FT-IR spectra, adsorption isotherms and interpretation thereof, contact angle measurements, scheme of the fixed-bed reactor setting, breakthrough curves and interpretation thereof, NMR spectra and interpretation thereof (PDF)

DFT-relaxed structures of Al-TCPB (CIF)

DFT-relaxed structures of Al-TCPB(OH) (CIF)

DFT-relaxed structures of Al-TCPB(NH$_2$) (CIF)

■ AUTHOR INFORMATION

Corresponding Authors

Andrzej Gładysiak − *Materials Discovery Laboratory, Department of Chemistry, Oregon State University, Corvallis, Oregon 97331, United States;* ⓞ orcid.org/0000-0003-3302-1644; Email: andrzej.gladysiak@oregonstate.edu

Kyriakos C. Stylianou − *Materials Discovery Laboratory, Department of Chemistry, Oregon State University, Corvallis, Oregon 97331, United States;* ⓞ orcid.org/0000-0003-1670-0020; Email: kyriakos.stylianou@oregonstate.edu

Authors

Ah-Young Song − *Department of Chemical and Biomolecular Engineering, University of California, Berkeley, California 94720, United States; Materials Sciences Division, Lawrence Berkeley National Laboratory, Berkeley, California 94720, United States*

Rebecca Vismara − *Departamento de Química Inorgánica, Universidad de Granada, Granada 18071, Spain;* ⓞ orcid.org/0000-0001-9474-7671

Madison Waite − *Department of Chemical and Biomolecular Engineering, University of California, Berkeley, California 94720, United States; Materials Sciences Division, Lawrence Berkeley National Laboratory, Berkeley, California 94720, United States*

Nawal M. Alghoraibi − *Research and Development Center, ARAMCO, Dhahran 34466, Saudi Arabia*

Ammar H. Alahmed − *Research and Development Center, ARAMCO, Dhahran 34466, Saudi Arabia*

Mourad Younes − *Research and Development Center, ARAMCO, Dhahran 34466, Saudi Arabia*

Hongliang Huang − *State Key Laboratory of Separation Membranes and Membrane Processes, Tiangong University, Tianjin 300387, P. R. China; School of Chemical Engineering, Tiangong University, Tianjin 300387, P. R. China;* ⊙ orcid.org/0000-0001-9690-9259

Jeffrey A. Reimer − *Department of Chemical and Biomolecular Engineering, University of California, Berkeley, California 94720, United States; Materials Sciences Division, Lawrence Berkeley National Laboratory, Berkeley, California 94720, United States*

Complete contact information is available at:
https://pubs.acs.org/10.1021/jacsau.4c00923

Notes

The authors declare no competing financial interest.

■ REFERENCES

(1) Metz, B. *IPCC Special Report on Carbon Dioxide Capture and Storage*; Intergovernmental Panel on Climate Change, Cambridge University Press: Cambridge, 2005.

(2) Intergovernmental Panel on Climate Change. *Climate Change 2022—Impacts, Adaptation and Vulnerability: Working Group II Contribution to the Sixth Assessment Report of the Intergovernmental Panel on Climate Change*; Cambridge University Press: Cambridge, 2023.

(3) U.S. Department of Energy, Office of Energy Statistics, U.S. Energy Information Administration. DOE/EIA-0035(2023/2) Monthly Energy Review February 2023. https://www.eia.gov/totalenergy/data/monthly/ (accessed Oct 15, 2024).

(4) Schmitt, T.; Leptinsky, S.; Turner, M.; Zoelle, A.; White, C. W.; Hughes, S.; Homsy, S.; Woods, M.; Hoffman, H.; Shultz, T.; James, R. E. *Cost and Performance Baseline for Fossil Energy Plants Vol. 1: Bituminous Coal and Natural Gas to Electricity*: United States, 2022.

(5) Rochelle, G. T. Amine Scrubbing for CO_2 Capture. *Science* 2009, 325 (5948), 1652−1654.

(6) Huck, J. M.; Lin, L.-C.; Berger, A. H.; Shahrak, M. N.; Martin, R. L.; Bhown, A. S.; Haranczyk, M.; Reuter, K.; Smit, B. Evaluating different classes of porous materials for carbon capture. *Energy Environ. Sci.* 2014, 7 (12), 4132−4146.

(7) Carneiro, J. S. A.; Innocenti, G.; Moon, H. J.; Guta, Y.; Proaño, L.; Sievers, C.; Sakwa-Novak, M. A.; Ping, E. W.; Jones, C. W. Insights into the Oxidative Degradation Mechanism of Solid Amine Sorbents for CO_2 Capture from Air: Roles of Atmospheric Water. *Angew. Chem., Int. Ed.* 2023, 62 (24), No. e202302887.

(8) Burtch, N. C.; Jasuja, H.; Walton, K. S. Water Stability and Adsorption in Metal−Organic Frameworks. *Chem. Rev.* 2014, 114 (20), 10575−10612.

(9) Trickett, C. A.; Helal, A.; Al-Maythalony, B. A.; Yamani, Z. H.; Cordova, K. E.; Yaghi, O. M. The chemistry of metal−organic frameworks for CO_2 capture, regeneration and conversion. *Nat. Rev. Mater.* 2017, 2 (8), 17045.

(10) Bhatt, P. M.; Belmabkhout, Y.; Cadiau, A.; Adil, K.; Shekhah, O.; Shkurenko, A.; Barbour, L. J.; Eddaoudi, M. A Fine-Tuned Fluorinated MOF Addresses the Needs for Trace CO_2 Removal and Air Capture Using Physisorption. *J. Am. Chem. Soc.* 2016, 138 (29), 9301−9307.

(11) Shekhah, O.; Belmabkhout, Y.; Chen, Z.; Guillerm, V.; Cairns, A.; Adil, K.; Eddaoudi, M. Made-to-order metal-organic frameworks for trace carbon dioxide removal and air capture. *Nat. Commun.* 2014, 5 (1), 4228.

(12) Shekhah, O.; Belmabkhout, Y.; Adil, K.; Bhatt, P. M.; Cairns, A. J.; Eddaoudi, M. A facile solvent-free synthesis route for the assembly of a highly CO_2 selective and H_2S tolerant NiSIFSIX metal−organic framework. *Chem. Commun.* 2015, 51 (71), 13595−13598.

(13) Nugent, P.; Belmabkhout, Y.; Burd, S. D.; Cairns, A. J.; Luebke, R.; Forrest, K.; Pham, T.; Ma, S.; Space, B.; Wojtas, L.; Eddaoudi, M.; Zaworotko, M. J. Porous materials with optimal adsorption thermodynamics and kinetics for CO_2 separation. *Nature* 2013, 495 (7439), 80−84.

(14) McDonald, T. M.; Lee, W. R.; Mason, J. A.; Wiers, B. M.; Hong, C. S.; Long, J. R. Capture of carbon dioxide from air and flue gas in the alkylamine-appended metal-organic framework mmen-Mg_2(dobpdc). *J. Am. Chem. Soc.* 2012, 134 (16), 7056−7065.

(15) Gargiulo, N.; Pepe, F.; Caputo, D. CO_2 adsorption by functionalized nanoporous materials: a review. *J. Nanosci. Nanotechnol.* 2014, 14 (2), 1811−1822.

(16) Das, A.; D'Alessandro, D. M. Tuning the functional sites in metal−organic frameworks to modulate CO_2 heats of adsorption. *CrystEngComm* 2015, 17 (4), 706−718.

(17) Wang, H.; Peng, J.; Li, J. Ligand Functionalization in Metal−Organic Frameworks for Enhanced Carbon Dioxide Adsorption. *Chem. Rec.* 2016, 16 (3), 1298−1310.

(18) Sun, Z.; Liao, Y.; Zhao, S.; Zhang, X.; Liu, Q.; Shi, X. Research progress in metal−organic frameworks (MOFs) in CO_2 capture from post-combustion coal-fired flue gas: characteristics, preparation, modification and applications. *J. Mater. Chem. A* 2022, 10 (10), 5174−5211.

(19) Caskey, S. R.; Wong-Foy, A. G.; Matzger, A. J. Dramatic Tuning of Carbon Dioxide Uptake via Metal Substitution in a Coordination Polymer with Cylindrical Pores. *J. Am. Chem. Soc.* 2008, 130 (33), 10870−10871.

(20) McDonald, T. M.; Mason, J. A.; Kong, X.; Bloch, E. D.; Gygi, D.; Dani, A.; Crocella, V.; Giordanino, F.; Odoh, S. O.; Drisdell, W. S.; Vlaisavljevich, B.; Dzubak, A. L.; Poloni, R.; Schnell, S. K.; Planas, N.; Lee, K.; Pascal, T.; Wan, L. F.; Prendergast, D.; Neaton, J. B.; Smit, B.; Kortright, J. B.; Gagliardi, L.; Bordiga, S.; Reimer, J. A.; Long, J. R. Cooperative insertion of CO_2 in diamine-appended metal-organic frameworks. *Nature* 2015, 519 (7543), 303−308.

(21) Lancheros, A.; Goswami, S.; Mian, M. R.; Zhang, X.; Zarate, X.; Schott, E.; Farha, O. K.; Hupp, J. T. Modulation of CO_2 adsorption in novel pillar-layered MOFs based on carboxylate−pyrazole flexible linker. *Dalton Trans.* 2021, 50 (8), 2880−2890.

(22) Yazaydın, A. Ö.; Benin, A. I.; Faheem, S. A.; Jakubczak, P.; Low, J. J.; Willis, R. R.; Snurr, R. Q. Enhanced CO_2 Adsorption in Metal-Organic Frameworks via Occupation of Open-Metal Sites by

Coordinated Water Molecules. *Chem. Mater.* **2009**, *21* (8), 1425−1430.

(23) González-Martínez, G. A.; Zárate, J. A.; Martínez, A.; Sánchez-González, E.; Álvarez, J. R.; Lima, E.; González-Zamora, E.; Ibarra, I. A. Confinement of alcohols to enhance CO_2 capture in MIL-53(Al). *RSC Adv.* **2017**, *7* (40), 24833−24840.

(24) González-Zamora, E.; Ibarra, I. A. CO_2 capture under humid conditions in metal−organic frameworks. *Mater. Chem. Front.* **2017**, *1* (8), 1471−1484.

(25) Liao, P.-Q.; Chen, H.; Zhou, D.-D.; Liu, S.-Y.; He, C.-T.; Rui, Z.; Ji, H.; Zhang, J.-P.; Chen, X.-M. Monodentate hydroxide as a super strong yet reversible active site for CO_2 capture from high-humidity flue gas. *Energy Environ. Sci.* **2015**, *8* (3), 1011−1016.

(26) Song, B.-Q.; Yang, Q.-Y.; Wang, S.-Q.; Vandichel, M.; Kumar, A.; Crowley, C.; Kumar, N.; Deng, C.-H.; GasconPerez, V.; Lusi, M.; Wu, H.; Zhou, W.; Zaworotko, M. J. Reversible Switching between Nonporous and Porous Phases of a New SIFSIX Coordination Network Induced by a Flexible Linker Ligand. *J. Am. Chem. Soc.* **2020**, *142* (15), 6896−6901.

(27) Nikolayenko, V. I.; Castell, D. C.; Sensharma, D.; Shivanna, M.; Loots, L.; Forrest, K. A.; Solanilla-Salinas, C. J.; Otake, K.-i.; Kitagawa, S.; Barbour, L. J.; Space, B.; Zaworotko, M. J. Reversible transformations between the non-porous phases of a flexible coordination network enabled by transient porosity. *Nat. Chem.* **2023**, *15* (4), 542−549.

(28) Castell, D. C.; Nikolayenko, V. I.; Sensharma, D.; Koupepidou, K.; Forrest, K. A.; Solanilla-Salinas, C. J.; Space, B.; Barbour, L. J.; Zaworotko, M. J. Crystal Engineering of Two Light and Pressure Responsive Physisorbents. *Angew. Chem., Int. Ed.* **2023**, *62* (19), No. e202219039.

(29) Song, B.-Q.; Shivanna, M.; Gao, M.-Y.; Wang, S.-Q.; Deng, C.-H.; Yang, Q.-Y.; Nikkhah, S. J.; Vandichel, M.; Kitagawa, S.; Zaworotko, M. J. Shape-Memory Effect Enabled by Ligand Substitution and CO_2 Affinity in a Flexible SIFSIX Coordination Network. *Angew. Chem., Int. Ed.* **2023**, *62* (47), No. e202309985.

(30) Koupepidou, K.; Nikolayenko, V. I.; Sensharma, D.; Bezrukov, A. A.; Vandichel, M.; Nikkhah, S. J.; Castell, D. C.; Oyekan, K. A.; Kumar, N.; Subanbekova, A.; Vandenberghe, W. G.; Tan, K.; Barbour, L. J.; Zaworotko, M. J. One Atom Can Make All the Difference: Gas-Induced Phase Transformations in Bisimidazole-Linked Diamondoid Coordination Networks. *J. Am. Chem. Soc.* **2023**, *145* (18), 10197−10207.

(31) Li, X.; Sensharma, D.; Loots, L.; Geng, S.; Nikkhah, S. J.; Lin, E.; Bon, V.; Liu, W.; Wang, Z.; He, T.; Mukherjee, S.; Vandichel, M.; Kaskel, S.; Barbour, L. J.; Zhang, Z.; Zaworotko, M. J. Reversible Phase Transformations in a Double-Walled Diamondoid Coordination Network with a Stepped Isotherm for Methane. *J. Am. Chem. Soc.* **2024**, *146* (27), 18387−18395.

(32) Nikolayenko, V. I.; Castell, D. C.; Sensharma, D.; Shivanna, M.; Loots, L.; Otake, K.-i.; Kitagawa, S.; Barbour, L. J.; Zaworotko, M. J. Metal cation substitution can tune CO_2, H_2O and CH_4 switching pressure in transiently porous coordination networks. *J. Mater. Chem. A* **2023**, *11* (30), 16019−16026.

(33) Xu, F.; Yu, Y.; Yan, J.; Xia, Q.; Wang, H.; Li, J.; Li, Z. Ultrafast room temperature synthesis of GrO@HKUST-1 composites with high CO_2 adsorption capacity and CO_2/N_2 adsorption selectivity. *Chem. Eng. J.* **2016**, *303*, 231−237.

(34) Chen, Y.; Lv, D.; Wu, J.; Xiao, J.; Xi, H.; Xia, Q.; Li, Z. A new MOF-505@GO composite with high selectivity for CO_2/CH_4 and CO_2/N_2 separation. *Chem. Eng. J.* **2017**, *308*, 1065−1072.

(35) Salehi, S.; Anbia, M. High CO_2 Adsorption Capacity and CO_2/ CH_4 Selectivity by Nanocomposites of MOF-199. *Energy Fuels* **2017**, *31* (5), 5376−5384.

(36) Muschi, M.; Devautour-Vinot, S.; Aureau, D.; Heymans, N.; Sene, S.; Emmerich, R.; Ploumistos, A.; Geneste, A.; Steunou, N.; Patriarche, G.; De Weireld, G.; Serre, C. Metal−organic framework/ graphene oxide composites for CO_2 capture by microwave swing adsorption. *J. Mater. Chem. A* **2021**, *9* (22), 13135−13142.

(37) Emerson, A. J.; Chahine, A.; Batten, S. R.; Turner, D. R. Synthetic approaches for the incorporation of free amine function-alities in porous coordination polymers for enhanced CO_2 sorption. *Coord. Chem. Rev.* **2018**, *365*, 1−22.

(38) Khutia, A.; Janiak, C. Programming MIL-101Cr for selective and enhanced CO_2 adsorption at low pressure by postsynthetic amine functionalization. *Dalton Trans.* **2014**, *43* (3), 1338−1347.

(39) Kim, S.-N.; Kim, J.; Kim, H.-Y.; Cho, H.-Y.; Ahn, W.-S. Adsorption/catalytic properties of MIL-125 and NH2-MIL-125. *Catal. Today* **2013**, *204*, 85−93.

(40) Cmarik, G. E.; Kim, M.; Cohen, S. M.; Walton, K. S. Tuning the adsorption properties of UiO-66 via ligand functionalization. *Langmuir* **2012**, *28* (44), 15606−15613.

(41) Boyd, P. G.; Chidambaram, A.; García-Díez, E.; Ireland, C. P.; Daff, T. D.; Bounds, R.; Gładysiak, A.; Schouwink, P.; Moosavi, S. M.; Maroto-Valer, M. M.; Reimer, J. A.; Navarro, J. A. R.; Woo, T. K.; Garcia, S.; Stylianou, K. C.; Smit, B. Data-driven design of metal−organic frameworks for wet flue gas CO_2 capture. *Nature* **2019**, *576* (7786), 253−256.

(42) Loiseau, T.; Serre, C.; Huguenard, C.; Fink, G.; Taulelle, F.; Henry, M.; Bataille, T.; Férey, G. A Rationale for the Large Breathing of the Porous Aluminum Terephthalate (MIL-53) Upon Hydration. *Chem.—Eur. J.* **2004**, *10* (6), 1373−1382.

(43) Jansen, C.; Tannert, N.; Lenzen, D.; Bengsch, M.; Millan, S.; Goldman, A.; Jordan, D. N.; Sondermann, L.; Stock, N.; Janiak, C. Unravelling gas sorption in the aluminum metal-organic framework CAU-23: CO_2, H_2, CH_4, SO_2 sorption isotherms, enthalpy of adsorption and mixed-adsorptive calculations. *Z. Anorg. Allg. Chem.* **2022**, *648* (17), No. e202200170.

(44) Fan, W.; Wang, K.-Y.; Welton, C.; Feng, L.; Wang, X.; Liu, X.; Li, Y.; Kang, Z.; Zhou, H.-C.; Wang, R.; Sun, D. Aluminum metal−organic frameworks: From structures to applications. *Coord. Chem. Rev.* **2023**, *489*, 215175.

(45) Loughran, R. P.; Hurley, T.; Gładysiak, A.; Chidambaram, A.; Khivantsev, K.; Walter, E. D.; Graham, T. R.; Reardon, P.; Szanyi, J.; Fast, D. B.; Miller, Q. R. S.; Park, A.-H. A.; Stylianou, K. C. CO_2 capture from wet flue gas using a water-stable and cost-effective metal-organic framework. *Cell Rep. Phys. Sci.* **2023**, *4* (7), 101470.

(46) Chiu, N. C.; Loughran, R. P.; Gładysiak, A.; Vismara, R.; Park, A.-H. A.; Stylianou, K. C. Wet flue gas CO_2 capture and utilization using one-dimensional metal−organic chains. *Nanoscale* **2022**, *14* (40), 14962−14969.

(47) Krüger, M.; Siegel, R.; Dreischarf, A.; Reinsch, H.; Senker, J.; Stock, N. $[Al_2(OH)_2(TCPB)]$ − An Al-MOF based on a tetratopic linker molecule. *Microporous Mesoporous Mater.* **2015**, *216*, 27−35.

(48) Oktavian, R.; Goeminne, R.; Glasby, L. T.; Song, P.; Huynh, R.; Qazvini, O. T.; Ghaffari-Nik, O.; Masoumifard, N.; Cordiner, J. L.; Hovington, P.; Van Speybroeck, V.; Moghadam, P. Z. Gas adsorption and framework flexibility of CALF-20 explored via experiments and simulations. *Nat. Commun.* **2024**, *15* (1), 3898.

(49) Fan, D.; Naskar, S.; Maurin, G. Unconventional mechanical and thermal behaviours of MOF CALF-20. *Nat. Commun.* **2024**, *15* (1), 3251.

(50) Gładysiak, A.; Deeg, K. S.; Dovgaliuk, I.; Chidambaram, A.; Ordiz, K.; Boyd, P. G.; Moosavi, S. M.; Ongari, D.; Navarro, J. A. R.; Smit, B.; Stylianou, K. C. Biporous Metal−Organic Framework with Tunable CO_2/CH_4 Separation Performance Facilitated by Intrinsic Flexibility. *ACS Appl. Mater. Interfaces* **2018**, *10* (42), 36144−36156.

(51) Lin, J.-B.; Nguyen, T. T. T.; Vaidhyanathan, R.; Burner, J.; Taylor, J. M.; Durekova, H.; Akhtar, F.; Mah, R. K.; Ghaffari-Nik, O.; Marx, S.; Fylstra, N.; Iremonger, S. S.; Dawson, K. W.; Sarkar, P.; Hovington, P.; Rajendran, A.; Woo, T. K.; Shimizu, G. K. H. A scalable metal-organic framework as a durable physisorbent for carbon dioxide capture. *Science* **2021**, *374* (6574), 1464−1469.

(52) Akiyama, G.; Matsuda, R.; Sato, H.; Hori, A.; Takata, M.; Kitagawa, S. Effect of functional groups in MIL-101 on water sorption behavior. *Microporous Mesoporous Mater.* **2012**, *157*, 89−93.

(53) Xu, W.; Yaghi, O. M. Metal−Organic Frameworks for Water Harvesting from Air, Anywhere, Anytime. *ACS Cent. Sci.* **2020**, *6* (8), 1348−1354.

(54) Hanikel, N.; Pei, X.; Chheda, S.; Lyu, H.; Jeong, W.; Sauer, J.; Gagliardi, L.; Yaghi, O. M. Evolution of water structures in metal-organic frameworks for improved atmospheric water harvesting. *Science* **2021**, *374* (6566), 454−459.

(55) Lu, Z.; Duan, J.; Tan, H.; Du, L.; Zhao, X.; Wang, R.; Kato, S.; Yang, S.; Hupp, J. T. Isomer of NU-1000 with a Blocking c-pore Exhibits High Water−Vapor Uptake Capacity and Greatly Enhanced Cycle Stability. *J. Am. Chem. Soc.* **2023**, *145* (7), 4150−4157.

(56) Alawadhi, A. H.; Chheda, S.; Stroscio, G. D.; Rong, Z.; Kurandina, D.; Nguyen, H. L.; Rampal, N.; Zheng, Z.; Gagliardi, L.; Yaghi, O. M. Harvesting Water from Air with High-Capacity, Stable Furan-Based Metal−Organic Frameworks. *J. Am. Chem. Soc.* **2024**, *146* (3), 2160−2166.

(57) Ullah, S.; Tan, K.; Sensharma, D.; Kumar, N.; Mukherjee, S.; Bezrukov, A. A.; Li, J.; Zaworotko, M. J.; Thonhauser, T. CO_2 Capture by Hybrid Ultramicroporous TIFSIX-3-Ni under Humid Conditions Using Non-Equilibrium Cycling. *Angew. Chem., Int. Ed.* **2022**, *61* (35), No. e202206613.

(58) Siegelman, R. L.; Milner, P. J.; Forse, A. C.; Lee, J. H.; Colwell, K. A.; Neaton, J. B.; Reimer, J. A.; Weston, S. C.; Long, J. R. Water Enables Efficient CO_2 Capture from Natural Gas Flue Emissions in an Oxidation-Resistant Diamine-Appended Metal-Organic Framework. *J. Am. Chem. Soc.* **2019**, *141* (33), 13171−13186.

(59) Quan, W.; Holmes, H. E.; Zhang, F.; Hamlett, B. L.; Finn, M. G.; Abney, C. W.; Kapelewski, M. T.; Weston, S. C.; Lively, R. P.; Koros, W. J. Scalable Formation of Diamine-Appended Metal-Organic Framework Hollow Fiber Sorbents for Postcombustion CO_2 Capture. *JACS Au* **2022**, *2* (6), 1350−1358.

(60) Mohideen, M. I. H.; Pillai, R. S.; Adil, K.; Bhatt, P. M.; Belmabkhout, Y.; Shkurenko, A.; Maurin, G.; Eddaoudi, M. A Fine-Tuned MOF for Gas and Vapor Separation: A Multipurpose Adsorbent for Acid Gas Removal, Dehydration, and BTX Sieving. *Chem* **2017**, *3* (5), 822−833.